A Simple Method for Predicting Rocket Exhaust Smoke Visibility

Andrew C. Victor* and Stuart H. Breil†
Naval Weapons Center, China Lake, Calif.

Ambient light scattered from metal oxide particles in composite-propellant rocket exhausts makes the missile trail visible at long ranges. In the selection of propellant aluminum concentration, it is important to be able to predict the distance from which the exhaust no longer is visible. In this paper, a simple methodology, amenable to hand calculation, is presented for this purpose. The user need supply only the propellant aluminum concentration, missile velocity and altitude, and the rocket motor thrust level. The methodology predicts smoke trail dimensions, particle concentration as a function of location in the trail, sunlight and skylight scattering, background obscuration, and the range at which the trail may be detected visually for any atmospheric attenuation level. The entire calculation can be carried out with a scientific pocket calculator.

Nomenclature

A = weight percent Al in propellant
B = brightness or luminance, lm-m^{-2} – sr^{-1} [Eq. (15)]
B_0 = intrinsic background brightness
B_r = apparent background brightness
B_R = path luminance [(Eq. 11)]
C = concentration
C_0 = intrinsic contrast
C_R = apparent contrast
d = plume diameter, m
D_x = dilution of particle concentration at x
f = mass fraction of gaseous jet effluent in exhaust plume
F = thrust of rocket motor, kN
i = Mie function
I_s = solar illuminance (sea-level value on clear day with sun at zenith is 1.24×10^5 lm-m^{-2})
K = ratio of horizon sky brightness to B_0
m = complex refractive index
n = particle concentration, m^{-3}
P = pressure, atm
Q_s = scattering efficiency
r = radial position in plume, m
r_s = particle radius, m
r_μ = particle radius, μm
R = range, km
T = temperature, K
u = plume gas mean velocity, m-sec^{-1}
V = scattering coefficient defined by Eqs. (13, 14, and 16)
x = longitudinal position in plume, m
X = longitudinal coordinate in Von Mises plane [Eq. (3)]
Y = radial coordinate in von Mises plane, [Eq. (4)]
ϵ = liminal contrast
ϵ_R = liminal contrast modified for range [Eq. (22)]
ρ = gas density
σ = atmospheric attenuation coefficient, km^{-1}
ϕ = weight percent Al_2O_3 in plume ar radius r_j

Subscripts

b = refers to plume directly below observer
c = plume centerline value
e = freestream value
h = refers to plume at observer's altitude (i.e., on horizon)
i = refers to interception term in contrast calculation
j = plume starting-point value
L = refers to a Lambert scatterer
sky = refers to skylight scattering from plume
sun = refers to sunlight scattered from plume
z = refers to plume at zenith
½ = value at half-velocity radius of plume

Received Feb. 14, 1977; revision received April 28, 1977.
Index categories: Jets, Wakes, and Viscid-Inviscid Flow Interactions; Solid and Hybrid Rocket Engines; Missile Systems.

*Physicist, Propulsion Development Department. Associate Fellow AIAA.
†Physicist, Propulsion Development Department.

Introduction

THE presence of smoke in rocket exhaust trails is of interest from two main points of view. First, visibility of a smoke trail may provide advance warning of an approaching missile and may provide the enemy with a means of locating the launch site. Second, attenuation by a smoky exhaust may make line-of-sight optical guidance systems unworkable. It is therefore important to be able to select propellants whose levels of smoke are low enough to avoid either of these problems.

Attenuation of light by exhaust smoke is analytically the simpler of the two problems. It is not dealt with specifically in this paper. However, it is included as part of the interception term in the visibility model.

Exhaust smoke can be treated in two categories. The primary smoke, composed of the particulate matter expelled from the motor, which is the major offender when it is present in substantial concentrations, is the concern of this paper. The secondary smoke, resulting from condensation and growth of water and water-solution droplets, becomes important only when the primary smoke effects are negligible. Although primary smoke particles can be assumed to undergo no changes in size distribution after leaving the rocket nozzle, secondary smoke particles form in regions of the exhaust which have cooled below the dew point for the local water and water-solute mixtures. Since the treatment of secondary smoke requires inclusion of droplet growth and coagulation kinetics, its analytical treatment is more complicated than primary smoke and was not included in this study. Theoretical and experimental studies of secondary smoke are in progress, however, and, when reasonable secondary smoke particle size distributions have been identified, the methodology presented here will be adaptable readily to calculations of secondary smoke trail visibility.

Although there is no extensive literature on the subject of this paper, the supporting research areas of plume modeling, aluminum oxide particle size determination, light scattering, and meteorological visibility have been reported in hundreds

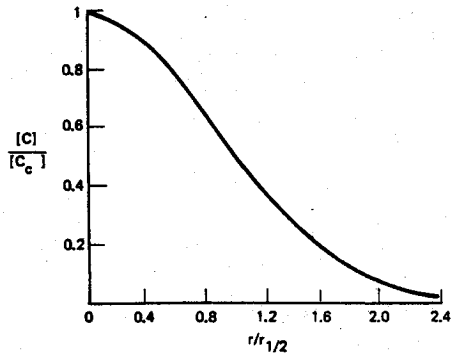

Fig. 1 Distribution of jet effluent concentration at an axial location in plume.

of writings. Those used in support of this study are referenced where their use was critical to development of the methodology.

The format of this paper is tutorial. In each section, the results are given as closed-form equations, tables, or graphs that are used in the final section to demonstrate application of the methodology. Starting with known values of propellant aluminum or aluminum oxide concentration, rocket motor thrust, and missile velocity and altitude, the methodology has tools for calculating the smoke trail dimensions, the concentration of particles at different positions in the exhaust, the scattering of light by these particles, the visual contrast of the plume to any background, and, finally, the range at which the smoke trail will fade from visibility.

Determination of Plume Starting Conditions

It is assumed that aluminum (Al) in the propellant is oxidized fully to aluminum oxide (Al_2O_3) in the motor chamber. Therefore, all Al_2O_3 present at the exit of the motor nozzle still is present farther downstream in the exhaust plume. Since the mass ratio of plume Al_2O_3 to propellant Al is simply the ratio of their molecular weights,

$$\phi = 1.89A \tag{1}$$

where ϕ and A are the weight percentages of Al_2O_3 at the starting position of the plume (where the plume radius is r_j) and Al in the propellant, respectively.

The dimensions of the plume near the nozzle exit expanded to atmospheric pressure are approximately proportional to the square root of the motor thrust level F and to the reciprocal of the square root of the ambient pressure P_e. For expediency, one may use the standard relationships for isentropic expansion[1] and for plume flow[2] to obtain the following approximate expression for the initial radius of the plume, in meters:

$$r_j = 0.02\sqrt{F/P_e} \tag{2}$$

where thrust is in kilonewtons (1 kN = 225 lb); and pressure is in atmospheres. Within this initial radius, the plume contains only jet effluent; no air has mixed in at this point. This approximate equation is based on the assumptions that plume chamber pressure = 68 atm, ratio of specific heats = 1.2, thrust coefficient = 1.67, and the nozzle half-angle = 15°.

Plume Model

The simple model of the plume used in this analysis is based on a linearized model[3,4] of Libby's theoretical analysis which assumes unity Prandtl and Schmidt numbers. The model has shown good agreement with centerline velocity and pressure data,[3-6] and, when coupled with the Naval Weapons Center equilibium chemistry model (PEP, propellant evaluation program[7]), it has predicted microwave attenuation quite accurately for a number of composite propellant plumes.[8] The weaknesses of the model become obvious for situations in which the chemical reactons are slow to reach equilibrium and a kinetic model is needed.[9] The model also employs a constant coefficient of eddy viscosity throughout the plume length. Recent studies have shown that this is a weakness, especially in chemical reacting plumes.[10-12] In this paper, we are interested only in plume regions downstream of the afterburning region. The linearized model is believed to be adequate for the present purpose of determining half-velocity radius ($r_{1/2}$) as a function of longitudinal position x in these regions. The half-velocity radius is defined as the radius at which the plume gas velocity is given by $(u_{1/2}+u_c)/2$.

It is assumed that all of the particles in the plume at any longitudinal position are contained within the boundary, which contains 90% of the gas flow. That this boundary is about 1.4 $r_{1/2}$ can be determined by integrating the curve in Fig. 1.[13] In the scattering calculations, the particles are assumed to be distributed uniformly within this boundary. Thus the boundaries of the visible plume can be obtained easily by determining $r_{1/2}$ as a function of x. The mathematical model for obtaining this relationship, derived from Libby's paper, is

$$x/r_j = 40X\rho_j/\rho_c u_j/(u_c-u_e)(r_j/r_{1/2}) \tag{3}$$

$$r_{1/2}/r_j = (\rho_j u_j/\rho_c u_{1/2})^{1/2} Y_{1/2} \tag{4}$$

where

$Y_{1/2} = 1.49 + 0.35X - 0.0057X^2$ (for $X<30$)

$Y_{1/2} = 5.5 + 0.047X$ (for $X>30$)

$\rho_j/\rho_c = T_c/T_j$, static temperatures

$T_c = [f_c + T_e/(T_j-T_e)](T_j-T_e)$, stagnation temperatures

$u_c = [f_c + u_e/(u_j-u_e)](u_j-u_e)$

$u_{1/2} = (u_e+u_c)/2$

where $f_c = 0.3/X$, based on detailed analysis of the Libby model at $r_{1/2}$.

For composite propellants, $T_j = 2000$ K is a reasonable assumption.[8] The variable f_c is the mass fraction of jet gas on

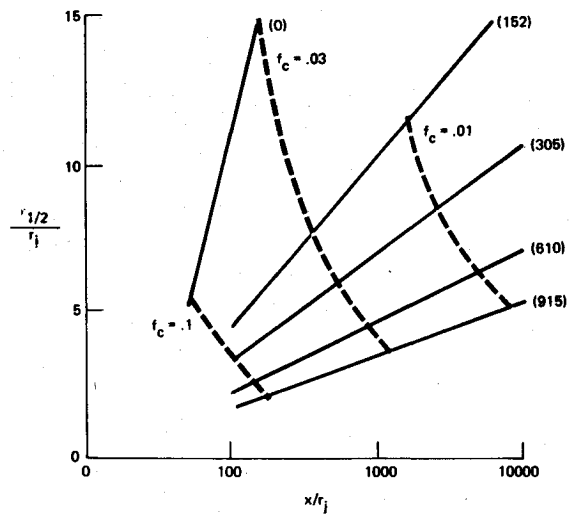

Fig. 2 Calculated variation of half-velocity radius with downstream plume position and missile velocity. Typical values of f_c used in the calculation are shown. (Numbers in parentheses are missile velocity, u_e, m-sec^{-1}) $T_e = 300$°K, $T_j = 2000$ K, $u_j = 3000$ m/sec.

the centerline of the plume at x. The plume outline is computed by determing $r_{1/2}/r_j$ and x/r_j for selected values of f_c. For downstream smoke trail calculations, values of f_c less than 0.1 are of interest. Figure 2 is a convenient display of the calculated variation of $r_{1/2}$ with x for several values of missile velocity u_e. Photographs of static motor firings and of supersonic missile flights confirm the general correctness of the model.

Consistent with the assumption that the radius of the smoke trail is 1.4 $r_{1/2}$, the dilution of particle concentration at x is approximately

$$D_x = [C_x]/[C_j] = \tfrac{1}{2}\,(r_j/r_{1/2})^2 \tag{5}$$

where $[C_j]$ is the concentration of particles at the initial plume radius r_j.

Particle Model

Early studies indicated that the size distribution of Al_2O_3 in rocket motor exhausts peaked near 3 μ.[14,15] More recent work has shown that most of the particles are very small, with a mode radius around 0.05 μm.[16,17] The distribution measured by Kraeutle[17] shows that, although 50% of the particles have radii less than 0.1 μm, 50% of the particle mass is contained in particles larger than 2.8 μm. For light scattering calculations, Kraeutle's distribution can be approximated by (for particles-m^{-3})

$$n_K(r) = 1.11\times 10^{22} r_\mu^4 \exp(-35.9 r_\mu^{0.5}) + 5.33\times 10^{13} r_\mu^3 \exp(-6 r_\mu) \tag{6}$$

Dawborn's distribution is given by

$$n_D(r) = 2.24\times 10^{15} r_\mu^3 \exp(-82.54 r_\mu) + 1.12\times 10^{11} r_\mu^2 \exp(-14.85 r_\mu^{0.5}) \tag{7}$$

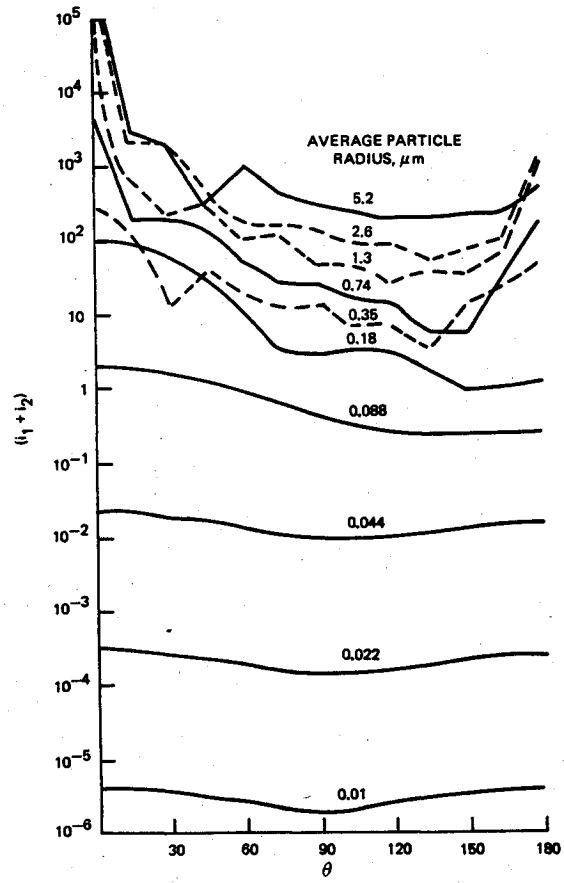

Fig. 3 Calculated Mie functions for Al_2O_3 particles with refractive index $m = 1.71\text{-}0.01\,i$.

where $n(r)$ represents the number of particles of radius r_μ (in $\mu m = 10^{-6}$ m units) in 1 m^3 of gas containing 1 wt% Al_2O_3. At this concentration, the plume contains 5.9×10^{-7} m^3-particles/m^3 gas, assuming solid spherical particles and $\rho_j = 2.3\times 10^{-4}$ g-cm^{-3} (which is a result of some detailed independent plume calculations). The integral of $n(r)$ over all values of r gives the total number of particles per cubic meter of the plume, N. Deirmendjian[18] gives a simple method for calculating N and the total particle volume from $n(r)$. For Al_2O_3 concentrations other than 1% it is assumed that the particle distribution is given by $n(r)\phi$.

Dawborn's distribution has many more small particles than Kraeutle's. Since the data for the Dawborn distribution were obtained by sampling the plume of a very large missile about 12 min after it had flown by, it is likely that many of the larger particles had fallen out of the plume and were not collected. As a result, the Dawborn distribution has over 100 times more particles. Kraeutle's distribution has been used as the basis for the rest of this paper, since it is based on laboratory data obtained under controlled, reproducible conditions.

Mie Scattering Functions

Since the visibility of smoky trails is due to scattering of incident light by particles, we next must determine the properties of light scattered by the particle distribution. The intensity of scattered light will vary with particle size and shape, particle refractive index, and scattering angle. (The scattering angle is defined as 0° if we are looking directly at the source through the scatterer and as 180° for backscattering, with the source behind the observer.) Therefore, scattering functions must be determined over the range of particle sizes within the distribution and for scattering angles between 0° and 180°. The Mie functions define the necessary properties. The Mie functions are well described in a number of classic texts[18-20] The Mie calculations for this study were performed with a computer program developed by Bird of the Naval Weapons Center.[21]

The scattering properties were examined for spherical particles between 0.0036 and 7.2 μm radius in eleven subgroups, each containing a particle size range in which the largest particle was just twice the radius of the smallest. It was assumed that the scattering of visible light can be well approximated by the scattering of a single wavelength, 0.55 μm. This is a reasonable assumptions because of the filtering action of the human eye.[22] The relative sensitivity of the eye drops to 10% or its 0.55-μm value at 0.45 and 0.65 μm.

There is some uncertainty about the refractive index of Al_2O_3. The refractive index was assumed to be $M = 1.71 - 0.01\,i$ (where i indicates the imaginary unit vector) for the scattering functions shown in Fig. 3 which are used throughout the paper.[23] The imaginary term in the refractive index represents about 10 times greater absorption than has been reported for pure alumina crystals.[24]

Visibility Model

The visibility model of Jarman and De Turville[25] forms the basis for the visibility calculations performed in this study. The eye perceives objects because of their contrast with the background. The contrast will be in terms of brightness and color. In this paper, the effect of color is ignored.

The inherent contrast between an object of brightness B and its background of brightness B_0 is given by[26]

$$C_0 = (B - B_0)/B_0 \tag{8}$$

As one moves away from the object, the apparent contrast is decreased by atmospheric absorption:

$$C_R = C_0 (B_0/B_r) e^{-\sigma R} \tag{9}$$

The atmospheric attenuation coefficient σ is given in Fig. 4. The apparent brightness of the background is $B_r = B_0 e^{-\sigma R}$

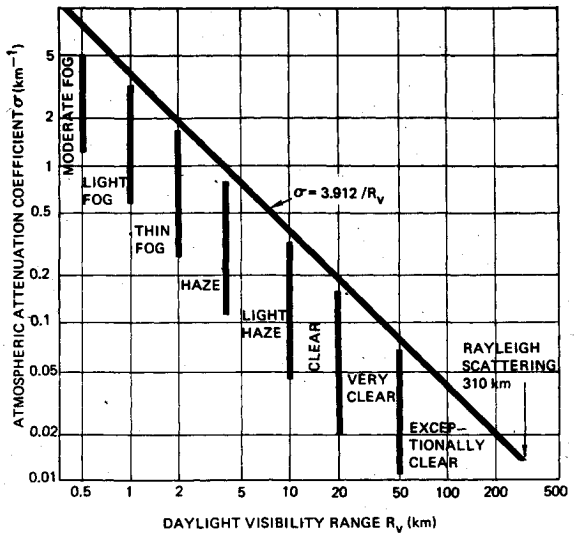

Fig. 4 Atmospheric attenuation coefficient for visible light (extinction coefficient) as a function of daylight visibility range (sometimes called "visibility" or "meteorological range").

$+B_R$. The path luminance B_R adds the sun and skylight scattered along the transmission path to the apparent intensity of the background and the object. Thus,

$$C_R = C_0(1 + B_R e^{\sigma R}/B_0)^{-1} \tag{10}$$

The path luminance is given approximately by

$$B_R = KB_0(1 - e^{-\sigma R}) \tag{11}$$

where K is the ratio of horizon sky brightness to background brightness. In sunlight, values of K for typical backgrounds are 0.2 for snow, 1 for desert, 3 for zenith sky, and 5 for forest. Under an overcast sky $K = 1$ for snow, 1 for zenith sky, 7 for desert, and 25 for forest.[22] Ocean background values of K can vary from about 1-3 for rough seas to 5 or more for smooth seas under a clear sky and are about 1 or less under an overcast sky.

There is a liminal contrast or threshold of visual contrast ϵ. When the apparent contrast of an object against a background is lower than the liminal contrast for an object of that apparent size (angle subtended at the eye), the object cannot be distinguished from the background. The liminal contrast increases with decreasing apparent size of the object. Thus the factors that cause an object to fade from view as it recedes from the eye include both its decreasing contrast and the increasing liminal contrast.

The perceived brightness of a plume derives from three effects: 1) sunlight scattered into the eye by the plume (B_{sun}); 2) skylight scattered into the eye by the plume (B_{sky}); and 3) that part of the background light reaching the eye after transmission through the plume (B). Thus, Eq. (8) for plume brightness B_p can be expanded to

$$C_0 = (B_P/B_0) - 1 = B_{sun}/B_0 + B_{sky}/B_0 + B/B_0 - 1 \tag{12}$$

When sunlight of intensity I_s falls on a single particle, the intensity of scattered light is $I_s(i_1 + i_2)/2\ (2\pi/\lambda)^2 R^2$ at a distance R.[19] The Mie function $(i_1 + i_2)$, shown in Fig. 3, depends on the angle through which the sunlight is scattered. From Jarman and de Turville, scattering from a plume of depth or thickness d may be written as

$$\frac{B_{sun}}{B_0} = \left\{\left(\frac{\lambda}{2\pi}\right)^2 \frac{\sum n(i_1 + i_2)}{2}\right\} \frac{I_s}{B_0} \mathrm{d}\phi D_x = V_{sun} \frac{I_s}{B_0} \mathrm{d}\phi D_x \tag{13}$$

Table 1 Calculated values of visibility coefficients based on scattering model of Fig. 3

$\lambda = 0.55\ \mu$m

$n(r) = 1.11 \times 10^{22} r^4 \exp(-35.9r^{0.5}) + 5.33 \times 10^{13} r^3 \exp(-6r)$, m^{-3}

$$N = \sum_{r=0.007\mu m}^{7.2} n = 2.5 \times 10^{12} \text{ particles-m}^3$$

$$(Q_s)_{\text{eff}} = \sum nr_s^2 Q_s / \sum nr_s^2 = 1.57$$

Coefficient	Scattering angle, deg					
	15	30	60	90	135	180
V_{sun}	0.48	0.26	0.076	0.036	0.014	0.34
V_i	−0.93 (no dependence on θ, K, or I_s/B_0)					

	Sky only	Over desert $K=1$ (including Earth albedo)	Over snow $K=0.2$ (including Earth albedo)
V_{sky_z}	0.76	0.91	1.51
V_{sky_h}	0.46	0.91	2.76
V_{sky_b}	0.15	0.91	2.95

where the summation is over all particle sizes. The term within braces represents the scattering coefficient for a plume section of 1-m^2 cross section and 1 m-depth, containing 1 wt% Al_2O_3.

The skylight scattered to the eye by the plume is found by an extension of the previous treatment for sunlight scattering. Since light from 2π sr of sky (a hemisphere) is scattered to the eye, we must integrate over the whole sky, of variable brightness, $B'(\omega)$ and all angles of scattering. Jarman and de Turville give

$$\frac{B_{sky}}{B_0} = \left(\frac{\lambda}{2\pi}\right)^2 \frac{d}{2B_0} \sum n \int_{\text{all sky}} (i_1 + i_2) B'(\omega) \mathrm{d}\omega$$

Evaluation of the integral is complicated because the sky brightness varies with angle,[27] but for simplicity we can consider only skies of uniform brightness $B' = KB_0$. Since $\omega = 2\pi \sin\theta \mathrm{d}\theta$,

$$\left(\frac{B_{sky}}{B_0}\right)_z = \left\{\left(\frac{\lambda}{2\pi}\right)^2 \pi \sum n \int_0^{\pi/2} (i_1 + i_2) \sin\theta \mathrm{d}\theta\right\} K \mathrm{d}\phi D_x$$

$$= V_{sky_z} K \mathrm{d}\phi D_x \tag{14a}$$

for a plume at the zenith,

$$\left(\frac{B_{sky}}{B_0}\right)_h = \left\{\left(\frac{\lambda}{2\pi}\right)^2 \frac{\pi}{2} \sum n \int_0^{\pi} (i_1 + i_2) \sin\theta \mathrm{d}\theta\right\} K \mathrm{d}\phi D_x$$

$$= (V_{sky_z} + V_{sky_b})(K/2) \mathrm{d}\phi D_x \tag{14b}$$

for a plume at the horizon, and

$$\left(\frac{B_{sky}}{B_0}\right)_b = \left\{\left(\frac{\lambda}{2\pi}\right)^2 \pi \sum n \int_{\pi/2}^{\pi} (i_1 + i_2) \sin\theta \mathrm{d}\theta\right\} K \mathrm{d}\phi D_x$$

$$= V_{sky_b} K \mathrm{d}\phi D_x \tag{14c}$$

for a plume directly below the observer.

A similar set of terms should be included to account for scattering of the Earth albedo by the plume. Over desert, the scattering of albedo will be about as great as sky scattering. When Eq. (14a) applies to sky scattering, Eq. (14c) applies to Earth albedo scattering, and vice versa. Equation (14b) will apply to both sky and Earth light scattering simultaneously. For a snow-covered Earth, the Earth light will be about five times greater than skylight, and hence scattering of the Earth's albedo will be the more important term. In the rest of this discussion, we neglect the Earth albedo with the warning that it should be considered for accurate solution of particular problems. The effect of albdeo in one case is shown for comparison in Table 1.

The volume of particles comprising the plume smoke trail intercepts some of the background light incident on it. A uniform cloud of depth d containing n particles per unit volume, each of cross section πr_s^2 and having a scattering efficiency of Q_s, reduces the background brightness from B_0 to B, where

$$B=\exp(-n\pi r_s^2 Q_s d)B_0 \tag{15}$$

For a variety of particle sizes,

$$B/B_0=\exp(-d\pi\sum nr_s^2 Q_s)$$

Thus the interception term in the plume contrast expression, Eq. (12), becomes

$$B/B_0-1=\exp\left[\left\{\left(-\pi\sum nr_s^2 Q_s\right)\right\}\mathrm{d}\phi D_x\right]-1$$

For values of the exponent less than 0.5, we can use Eq. (16) instead, with less than 10% error:

$$B/B_0-1=-\left\{\pi\sum nr_s^2 Q_s\right\}\mathrm{d}\phi D_x=V_i\mathrm{d}\phi D_x$$

$$=-1 \text{ in the limit of an opaque plume} \tag{16}$$

Assuming that the same particle size distribution applies to all plumes containing Al_2O_3, regardless of concentration, the contrast (visibility) is only a function of scattering angle, plume radius [$d=2.8\ r_j$, $D_x=0.5\ (r_j/R_{1/2})^2$], and ϕ, the weight percent of Al_2O_3, so that $C_0=G(\theta)\mathrm{d}\phi D_x$, where $G(\theta)=V_{\mathrm{sun}}I_s/B_0+KV_{\mathrm{sky}}+V_i$ is called the "normalized contrast," and

$$C_0=1.4(r_j/R_{1/2})^2 r_j\phi G(\theta)=0.028\sqrt{F/P_e}(r_j/r_{1/2})^2\phi G(\theta) \tag{17}$$

The value of $G(\theta)$ varies with viewing angle and also has a slight dependence on whether the plume is at the zenith, the horizon, or below the observer.

The previous equations describe the plume contrast only if the assumption of single scattering applies. If the particle density is too great, the plume is "optically thick," and multiple scattering occurs. That is, a significant amount of the light scattered out of the plume by particles was scattered to those particles by other particles instead of arriving directly from outside the plume. The effect of multiple scattering is generally to redirect the angular distribution of scattered light, decreasing the forward scattering and increasing the backscattering. For materials with a complex refractive index (absorbing materials), multiple scattering also will decrease the integrated intensity of the scattered light. If the value of B/B_0 calculated in Eq. (15) is less than about 0.75, it is necessary to consider the effects of multiple scattering.[25]

Bauer[28] suggests that the multiple scattering by large clouds that are optically thick can be approximated by a Lambert's law reflector.[19] In this case, the sunlight scattering term

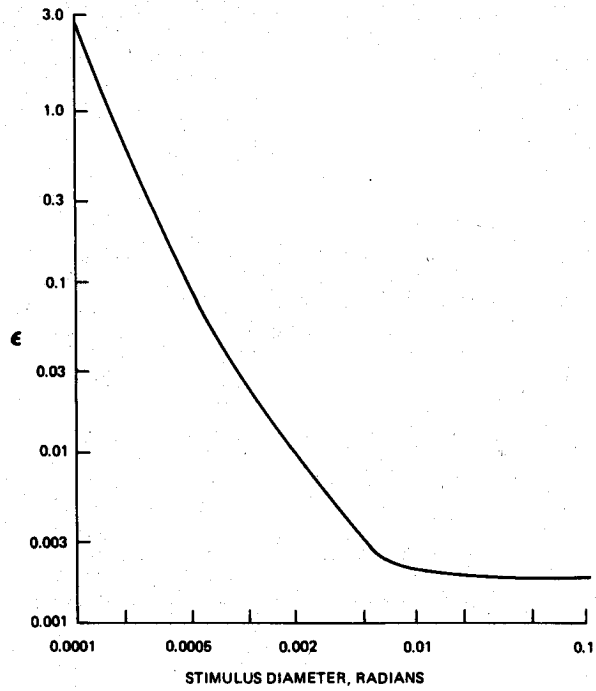

Fig. 5 Liminal contrast ϵ of circular objects for daylight viewing.

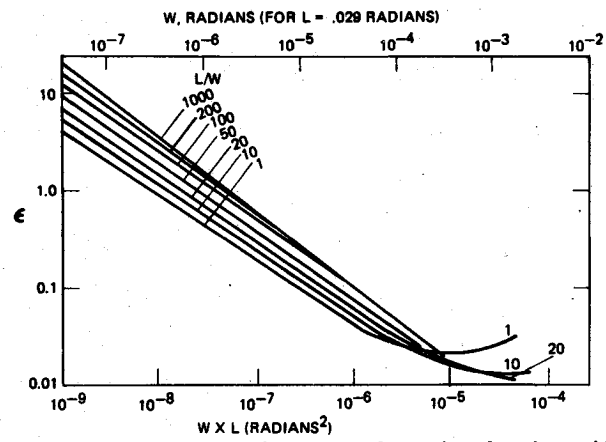

Fig. 6 Liminal contrast ϵ of rectangles for various length-to-width ratios for daylight viewing.

becomes

$$(B_{\mathrm{sun}}/B_0)_L=(I_s/4B_0)8/3(\sin\theta-\theta\cos\theta) \tag{18}$$

$$=0.0675(I_s/B_0)(\sin\theta-\theta\cos\theta)$$

The sky scattering term for a Lambert reflector also can be calculated, since

$$\frac{B_{\mathrm{sky}}}{B_0}=K\left(\frac{B_0}{I_s}\right)\int_{\mathrm{all\ sky}}\left(\frac{B_{\mathrm{sun}}}{B_0}\right)\sin\theta\mathrm{d}\theta$$

We obtain

$$(B_{\mathrm{sky}}/B_0)_{L_z}=0.6KB_0/I_s \tag{19a}$$

$$(B_{\mathrm{sky}}/B_0)_{L_n}=1.7KB_0/I_s \tag{19b}$$

$$(B_{\mathrm{sky}}/B_0)_{L_b}=4.8KB_0/I_s \tag{19c}$$

No light is transmitted through the Lambert scatterer, and very little light is scattered in forward directions. For scattering angles less than about 70°, the Lambert scatterer is

Table 2 Values of $G(\theta)$ calculated for typical situations

Function	Scattering angle, deg								Cloudy day (sky illumination only)
	15	30	60	90	135	180	I_s/B_0	K	
$G(\theta)_z$	9.43	5.03	1.35	0.55	0.11	6.63	20	1	$-0.17\,(K=1)$
	4.63	2.43	0.59	0.19	−0.16	3.23	10	1	
$G(\theta)_h$	9.12	4.72	1.05	0.25	−0.19	6.33	20	1	$-0.47\,(K=1)$
	4.33	2.13	0.29	−0.11	−0.46	2.93	10	1	
$G(\theta)_b$	...	...	7.42	3.42	1.22	33.8	100	5	$2.07\,(K=20)$

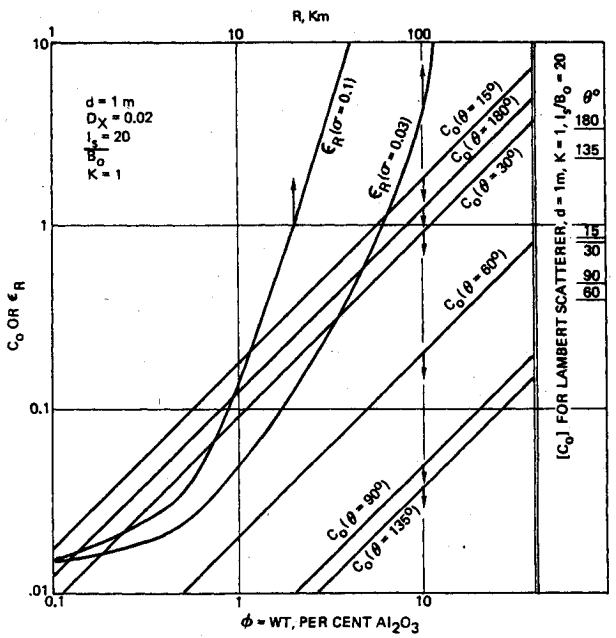

Fig. 7 Plume contrast and liminal contrast as a function of Al_2O_3 concentration and range.

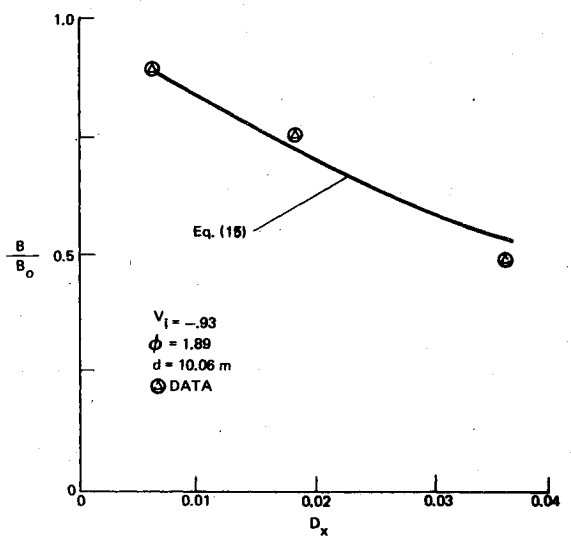

Fig. 8 Verification of the method by comparison with light-transmission data.

calculated to have negative contrast (i.e., appear darker than the sky background).

The criterion for conversion to Lambert scattering may be taken as

$$d\phi D_x > 0.32 \tag{20}$$

based on the criterion that $\exp(-V_l d\phi D_x) > 0.75$. This criterion will show a strong discontinuity in the conversion from single to multiple scattering. A less discontinuous criterion is to assume that the conversion to Lambertian scattering should be made when the backscattered light ($\theta = 180°$) from a single scattering medium equals that backscattered from a Lambertian scatterer. This gives the criterion

$$d\phi D_x = 0.62 \tag{21}$$

These two criteria together may mean that the conversion to Lambert scattering occurs over a factor of 2 change in the local optical thickness. Thus, for a plume of 1 m diam (d), the conversion between single scattering and multiple scattering, as calculable by the Lambert equations, occurs in the region where the local concentration of Al_2O_2 in the plume changes from 0.32 to 0.62 wt%.

Criteria for Visibility

When the plume visual contrast C_R is equal to the visual contrast threshold or liminal visibility ϵ, there is a 50% probability of detecting the plume. To obtain higher detection probabilities, the threshold contrast value used must be increased. To obtain detection probabilities of 0.7, 0.9, 0.95, and 0.99, one uses values of ϵ multiplied by 1.2, 1.5, 1.64, and 1.91, respectively.

The liminal contrast of a small object is a function only of the background brightness, object shape, and subtended area of the object as seen at the observer's eye. The effect of changes in background brightness is negligible over the range of brightness encountered in daylight observations.[29] For objects with a circular apparent cross section, the liminal contrast in daylight varies only with the stimulus diameter, as shown in Fig. 5. The stimulus diameter or subtended diameter in radians is just the plume diameter divided by range from eye to plume. The plume will appear circular in shape if it is observed along the plume axis. From observation points more than 5° off the plume axis, the plume shape is more rectangular.

Values of liminal contrast for objects subtending a rectangular cross section are shown in Fig. 6 for various length-to-width ratios and for a range of subtended areas covering five orders of magnitude.[30,31] The plume will appear approximately rectangular from all nonaxial vantage points. The effective length of the plume for visual detection is just the angle of the eye's foveal vision (0.029 rad).[32] Therefore, if the upper abscissal scale is read as the plume diameter d divided by the distance from the observer R, the liminal contrast is read easily for the appropriate plume length-to-width ratio (for which L still is taken to be 0.029 rad).

The use of Eq. (10) to obtain the apparent contrast of an object at a range R instead can be done reciprocally to obtain the range variation of liminal contrast while keeping C_0 constant. The effective liminal contrast of the plume is then

$$\epsilon_R = \epsilon[1 + K(e^{\sigma R} - 1)] \tag{22}$$

The criterion for 50% detection probability of the remote plume is $C_0 = \epsilon_R$. If C_0 is greater than ϵ_R, the plume will be

detected in more than 50% of attempted observations. The criterion for 90% detection probability is $C_0 = 1.5\,\epsilon_R$.

Application of the Methodology

In Table 1, numerical values for the various coefficients in the visibility model are given. These were calculated assuming the Mie functions of Fig. 3. The coefficients in Table 1 then may be used to calculate the values of the normalized contrast $[G(\theta)]$, for various operational situations. The operational environment is accounted for by including appropriate values of the ratio of solar illumination to background, I_s/B_0, and of the ratio of sky horizon to background brightness, K. The results of several such calculations are given in Table 2.

One only need use the values of $G(\theta)$ given in Table 2 in conjunction with Eq. (17) to calculate inherent contrast of Al_2O_3 containing plumes as a function of plume diameter d, particle dilution D_x, and wt% Al_2O_3, or any of the other combinations of parameters shown in Eq. (17). To demonstrate the technique, we have selected a case of horizontal viewing [i.e., $G(\theta)_h$ applies], with $I_s/B_0 = 20$ and $K = 1$. A dilution of $D_x = 0.02$ was selected as representative; it corresponds to $r_{1/2}/r_j = 5$. Figure 2 shows that this is in the range of plume radii which one expects to find in the downstream region, where plumes are likely to be detected. The plume diameter or depth d was chosen as 1 m to correspond to the plume of a 17.8-kN-thrust motor about 100 m downstream of the missile flying at about Mach 2. Sea-level ambient pressure was assumed. Equation (22) then was used to calculate the liminal contrast as a function of range for two conditions of atmospheric attenuation: $\sigma = 0.1$ km^{-1}, corresponding to a very clear day, and $\sigma = 0.03$ km^{-1}, corresponding to an exceptionally clear day.[22]

The results of the plume contrast calculations and the liminal contrast calculations both are plotted in Fig. 7. Figure 7 may be used in the following way: the intrinsic contrast is located as a function of ϕ on the straight line corresponding to the appropriate scattering angle. One then moves horizontally to intersect the appropriate curve for liminal contrast θ and then vertically upward to read the range for 50% detection probability on the upper abscissa. For example, a 1-m-diam plume containing 2% Al_2O_3 is calculated to be visible at just over 10 km for scattering angles of 180°, 15°, and 30° ($\sigma = 0.1$) At 60°, this plume is calculated to be visible at no more than 5-km range. The contrast calculated for a Lambert scatterer is shown along the right-hand edge of Fig. 7. The values of C_0 shown for the Lambert scatterer at 15°, 30°, and 60° correspond to negative contrasts. Using the relations of Eqs. (20) and (21) it would appear that for the plume characteristics considered in Fig. 7 the transition from single to Lambert scattering would occur between $\phi = 16$ and 31 or, for propellant aluminum percentages, between 8.5 and 16.5%.

In the region where single scattering applies, the calculated contrast of a plume will increase in direct proportion to increasing diameter. The liminal contrast ϵ_R will decrease roughly in inverse proportion to the changing plume diameter. Therefore, since a doubling of the plume diameter is calculated to cause a fourfold increase in visibility, all other things being equal, the visibility is prediced to vary directly as the motor thrust level.

The intrinsic contrast is strongly dependent on the particle size distribution model chosen and on the refractive index model chosen for Al_2O_3. Using a less absorptive refractive index for Al_2O_3[24] increases the predicted contrast by from 10 to 50%. Using the Dawborn particle distribution function [Eq. (7)] increases the predicted contrast by a factor of from 3 to 8. In combination, different choices of refractive index and particle distribution function can result in increases of five to ten times the predicted contrast. This generally increases the detection range predicted by ϵ_R by a factor of about 2.

Applied to a 1-m-diam plume, the methodology predicts that, to have a tactical missile plume that is not visible at more than 2-km range with exceptionally clear viewing conditions against a sky background, one is restricted to less than 0.4% Al in the propellant ($\phi = 0.7$). Viewed from above against a foliage background, the same size plume will be visible liminally if the propellant contains more than 0.02% aluminum.

Conclusions

The methodology presented in this paper suggests that the visibility of the exhaust trails of aluminim-containing propellants will depend on the operational situation in which they are observed. Although there are no visibility data to verify the methodology, there have been a number of light transmission measurements that could be used to evaluate part of the method by comparison with Eq. (15). For this purpose, the data for a rocket motor containing 1% Al fired into a well-stirred test chamber of 33.7 m^3 volume were chosen.[33] The total mass of a propellant was changed for different firings to give variations in dilution D_x. The excellent comparison of the data with Eq. (15) shown in Fig. 8 gives strong support to the assumptions concerning particle size distribution, the effects of dilution, the Mie calculations, and at least part of the contrast calculation.

Even in concentrations too low to be visible, primary smoke particles can act as nuclei for the condensation of secondary smoke. The condensation of water and water solutions of plume and atmospheric origins is an important aspect of the problem of rocket exhaust visibility. In many ways, it is identical to the problem of aircraft control formation, with the additional difficulties of solution chemistry. Further study of this problem is in progress. A flight-test measurement and analysis program on plume visibility is being pursued jointly by the Air Force, Army, and Navy.

Acknowledgment

This work was supported by the Naval Air Systems Command, Advanced Reliable Solid Propulsion Design Program, and the Naval Sea Systems Command, Plume Low Signature Requirements for Point/Area Defense Solid Propellant Motors Program.

References

[1] Sutton, G.P., *Rocket Propulsion Elements,* 3rd ed., Wiley, New York, 1963, Chap. 3.

[2] Love, E.S., Grigsby, C.E., Lee, L.P., and Woodling, M.J., "Experimental and Theoretical Studies of Axisymmetric Free Jets," NASA TR R-6, 1959.

[3] Victor, A.C. and Buecher, R.W., "An Analytical Approach to the Turbulent Mixing of Coaxial Jets," Naval Weapons Center, China Lake, Calif., NWC TP4070, Oct. 1966.

[4] Buecher, R.W. and Victor, A.C., "A Computer Program for the Calculation of Microwave Attenuation in a Rocket Exhaust," Naval Weapons Center, China Lake, Calif., NWC TP 4377, Oct. 1967.

[5] Libby, P.A., "Theoretical Analysis of Turbulent Mixing of Reactive Gases with Application to Supersonic Combustion of Hydrogen," *ARS Journal,* Vol. 32, March 1962, pp. 388-396.

[6] McCarten, R.M., "Measurements of Plume Velocity and Pressure Profiles," Naval Weapons Center, China Lake, Calif,, private communication, 1971.

[7] Cruise, D.R., "Notes on the Rapid Computation of Chemical Equilbria," *Journal of Physical Chemistry,* Vol. 68, Dec. 1964, pp. 3797-3802.

[8] Victor, A.C., "Plume Signal Interference, Part 1, Radar Attenuation," Naval Wespons Center, China Lake, Calif., NWC TP-5319, Pt. 1, June 1975.

[9] Mikatarian, R.R., Kau, C.J., and Pergament, H.S., "A Fast Computer Program for Non-Equilibrium Plume Predictions," Air Force Rocket Propulsion Lab., Edwards, Calif., AFRPL-TR-72-94, Aug. 1972.

[10] Jensen, D.E. and Wilson, A.S., "Predictions of Rocket Exhaust Flame Properties," *Combustion and Flame,* Vol. 25, Aug. 1975, pp. 43-55.

[11] Harsha, P.T., "Free Turbulent Mixing: A Critical Evaluation of Theory and Experiment," Arnold Air Force Station, Tullahoma, Tenn., AEDC-TR-71-36, Feb. 1971.

[12] "Free Turbulent Shear Flows, Vol. I, Conference Proceedings," NASA SP-321, July 1972.

[13] Boynton, F.P., "Composition in the Far Field of a Rocket Jet Mixing with Air," *Journal of Spacecraft and Rockets,* Vol. 3, June 1966, pp. 899-904.

[14] Rochelle, W.C., "Review of Thermal Radiation from Liquid and Solid Propellant Rocket Exhausts," NASA-TMX-53579, Feb. 1967.

[15] Worster, B.W. and Kadomiya, R.H., "Rocket Exhaust Aluminum Oxide Particle Properties," Aerodyne Research, Inc., Bedford, Mass., ARIRR-30, Aug. 1973.

[16] Dawborn, R. and Kinslow, M., "Studies of the Exhaust Products from Solid Propellant Rocket Motors," Arnold Air Force Station, Tullahoma, Tenn., AEDC-TR-76-49, Sept. 1976.

[17] Kraeutle, K.J., "Application of Particle Size Analysis in Combustin Research," AIAA Paper 77-978, Orlando, Fla., July 1977.

[18] Deirmendjian, D., *Electromagnetic Scattering on Spherical Polydispersions,* American Elsevier, New York, 1969, Chap. 3.

[19] Van de Hulst, H.C., *Light Scattering by Small Particles,* Wiley, New York, 1957.

[20] Kerker, M., *The Scattering of Light and Other Electromagnetic Radiation,* Academic Press, New York, 1969.

[21] Bird, R.E., "Calculation of Aerosol Particle Parameters from Measured Mie Scattering," Doctoral Dissertation, Brigham Young Univ., Provo, Utah, 1971.

[22] "Electro-Optics Handbook," 2nd ed., RCA Corp., Harrison, N.J., EOH-11, 1974.

[23] Dobbins, R.S. and Strand, L.D., "A Comparison by Two Methods of Measuring Particle Size of Al_2O_3 Produced by a Small Rocket Motor," *AIAA Journal,* Vol. 8, Sept.1970, pp. 1544-1550.

[24] Adams, J.M., "A Determination of the Emissive Properties of a Cloud of Molten Alumina Particles," *Journal of Quantitative Spectroscopy and Radiant Transfer,* Vol. 7, 1967, pp. 273-277.

[25] Jarman, R.T. and de Turville, C.M., "The Visibility and Length of Chimney Plumes," *Atmospheric Environment,* Vol. 3, 1969, pp. 257-280.

[26] Middleton, W.E.K., *Vision Through the Atmosphere,* Univ. of Toronto Press, Toronto, Canada, 1968.

[27] Duntley, S.Q., et al., "Visibility," *Applied Optics,* Vol. 3, May 1965, pp. 549-597.

[28] Bauer, E., "The Scattering of Infrared Radiation from Clouds," *Applied Optics,* Vol. 3, Feb. 1965, pp. 197-202.

[29] Blackwell, H.R., "Contrast Thresholds of the Human Eye," *Journal of the Optical Society of America,* Vol. 36, Nov. 1946, p. 624-643.

[30] Lamar, E.S., Hecht, S., Shlaer, S., and Handley, C.D., "Size, Shape, and Contrast in Detection of Targets by Daylight Vision. I. Data and Analytical Description, *Journal of the Optical Society of America,* Vol. 37, July 1947, pp. 531-545.

[31] Lamar, E.S., Hecht, S., Shaler, S., and Handley, C.D., "Size, Shape, and Contrast in Detection of Targets by Daylight Vision. II. Frequency of Seeing and the Quantum Theory of Cone Vision," *Journal of the Optical Society of America,* Vol. 38, Sept. 1948, pp. 741-755.

[32] Parker, J.F., "Bioastronautics Data Book," 2nd ed., NASA SP-3006, 1973, p. 628.

[33] Martin, K.I. and Viles, J.M., "Smoke Measurement Facility," Rohm and Hass Co., Huntsville, Ala., TR-S-159, March 1968.